

Zero-Shot Monocular Scene Flow Estimation in the Wild

Yiqing Liang^{1,2}

Abhishek Badki^{1*}

Hang Su^{1*}

James Tompkin²

Orazio Gallo¹

¹NVIDIA Research

²Brown University

arXiv:2501.10357v1 [cs.CV] 17 Jan 2025

Figure 1. Our model for monocular scene flow estimation predicts accurate pointmaps and 3D offsets for dynamic scenes from two input images (shown below each pane) captured by two cameras C_1 and C_2 at times t_1 and t_2 , respectively. The animation shows an interpolation of the pointmaps from C_1 at t_1 to C_2 at t_2 . These examples are from datasets not seen in training, showcasing the strong generalization abilities of our method. [Animated figures — Please click on each in Adobe Reader to play.]

Abstract

Large models have shown generalization across datasets for many low-level vision tasks, like depth estimation, but no such general models exist for scene flow. Even though scene flow has wide potential use, it is not used in practice because current predictive models do not generalize well. We identify three key challenges and propose solutions for each. First, we create a method that jointly estimates geometry and motion for accurate prediction. Second, we alleviate scene flow data scarcity with a data recipe that affords us 1M annotated training samples across diverse synthetic scenes. Third, we evaluate different parameterizations for scene flow prediction and adopt a natural and effective parameterization. Our resulting model outperforms existing methods as well as baselines built on large-scale models in terms of 3D end-point error, and shows zero-shot generalization to the casually captured videos from DAVIS and the robotic manipulation scenes from RoboTAP. Overall, our approach makes scene flow prediction more practical in-the-wild.

Release: https://research.nvidia.com/labs/zero_msf/. We will release the code and weights upon acceptance.

1. Introduction

Scene flow (SF) captures geometric transformations of dynamic scenes by the motion of points in 3D. As such, its accurate estimation can benefit applications like augmented reality [43], autonomous driving [21], and robotics [108]. Yet, despite its potential, it is not commonly used in practice. One contributing factor is the limited generalization ability of existing methods. This may be surprising given the progress of large-scale models [9] on other low-level vision tasks. For instance, the state-of-the-art approaches for tasks like image segmentation [41] and depth estimation (single and multi-view) [47, 102, 110, 111] lead benchmarks with impressive results.

Why is SF estimation different? We identify three critical challenges that hinder the generalization ability of feedforward SF estimation from monocular RGB videos.

* indicates equal contribution

First, geometry and motion are entangled, and thus require joint reasoning. That is because the 2D displacement we observe in image space is the combined effect of depth and motion, so an error in estimating either one will result in incorrect SF predictions. Even when predicting depth and motion jointly, estimating SF remains ill-posed because of the scale ambiguity, requiring effective learning to resolve it.

Second, good generalization requires training on large and diverse datasets, but labeled SF data are scarce. Further, some datasets are metric and some are in relative units, which can compromise learning if not properly accounted for. While this scale issue is well known in single-image depth estimation [79], it has not been addressed for SF estimation. Existing methods do not account for both of these factors, and therefore struggle to generalize to out-of-domain data.

Third, the estimation of SF is sensitive to the choice of parametrization. We find that, using depth + optical flow or taking the difference between the estimated 3D points before and after motion both compromise the quality of the results.

Based on these observations, we develop a new model for monocular SF estimation. We note that recent works in depth estimation like DUS_t3R [102] and MAS_t3R [47] show impressive generalization abilities for static scenes, but they do not model motion. To tackle the entanglement of geometry and motion, rather than using a separate network for motion, we extend them to predict offsets *jointly with geometry*, and train them for both tasks. Interestingly, we show that this joint training also improves their depth estimates for dynamic scenes, further supporting our observation that geometry and motion are entangled. To address the second challenge, we use datasets across several domains: indoors and outdoors, and with a diverse set of ground truth annotations. To help joint geometry and motion prediction quality, we use optical flow to supervise the projection of the SF in image space. Importantly, to exploit metric and relative datasets, we use a simple and scale-alignment mechanism across datasets. Finally, aware of the importance of parameterization choice, we study alternatives and propose to represent SF as pointmaps plus 3D motion offsets.

In evaluation against state-of-the-art monocular SF methods [30, 109] and Depth+Flow baselines, our approach improves both SF and geometry estimation in a zero-shot setting across both real and synthetic monocular SF estimation benchmarks. Figure 1 uses our SF and pointmap estimates to animate point motion over time. The quality of these results shows the zero-shot generalization ability of our method, since none of those datasets were used in training. This strong generalization ability is in contrast to existing SF estimation methods that have reduced performance on data not seen in training.

In summary, we introduce the first scene flow approach that leverages large-scale data for accurate, in-the-wild estimation. We show that joint training of geometry and motion

is central to its success, and that training for motion also helps depth estimation when the scene is dynamic. Not least, we describe a data and training strategy that is key to our method’s ability to learn from large data.

2. Related Work

2.1. Scene Flow Estimation

Scene flow (SF) estimation is the task of estimating 3D motion and geometry fields [93]. Often, works focus on the autonomous driving scenario, and few studies have been conducted on in-the-wild generalization.

Many SF estimation methods, including the earliest ones, assume explicit 3D structure information as input. It could be a calibrated stereo pair [3, 7, 29, 32, 34, 37, 44, 46, 58, 62, 63, 67, 72, 81–83, 93–97, 103, 104, 117], depth images [27, 28, 35, 56, 61, 64, 75, 76, 85, 88, 89, 114, 121] or 3D point clouds [1, 4, 5, 8, 14–18, 24, 26, 33, 38, 40, 42, 45, 48–53, 57, 59, 68–70, 73, 74, 90, 92, 98, 100, 101, 105, 107, 116, 118, 119]. Among point-cloud-based methods, the community has explored run-time optimization techniques for generalization [1, 16, 45, 51, 52, 73]. Despite improving accuracy, these techniques incur high computation costs.

Although we also leverage pointmaps in scene flow estimation, our approach is feedforward and therefore much more efficient.

2.2. Monocular Scene Flow Estimation

We tackle the more general problem where no 3D information is provided: monocular scene flow (MSF) estimation. MSF requires methods to estimate both SF and 3D structure from a sequence of monocular images, which is ill-posed by nature. Thus, many algorithms [10, 13, 54, 60, 80, 109, 112, 122] decompose the task into subproblems. The first MSF work, Mono-SF [10], assumes that piecewise planar surface elements and rigid bodies are enough to approximate autonomous driving scenes. Optical-Expansion-based methods [54, 109] upgrade 2D optical flow to 3D scene flow. Multi-task approaches [13, 60, 80, 112, 122] jointly predict depth, optical flow, and camera motion.

These methods produce scene flow that is limited in accuracy due to the strong assumptions made, and are surpassed by Self-Mono-SF [30], the first MSF method to predict 3D motion vectors directly alongside depth. After Self-Mono-SF [30]’s success, later works devote to improving it. Multi-Mono-SF [31] extends it into multi-frame setting; RAFT-MSF [6] uses recurrent structure to enhance performance; EMR-MSF [36] applies ego-motion rigidity prior to further boost accuracy.

Despite the progress made, the methods largely focus on autonomous driving scenarios and only show very limited generalization capabilities to scenes out of that domain [31]. Our method shows superior in-domain performance and also

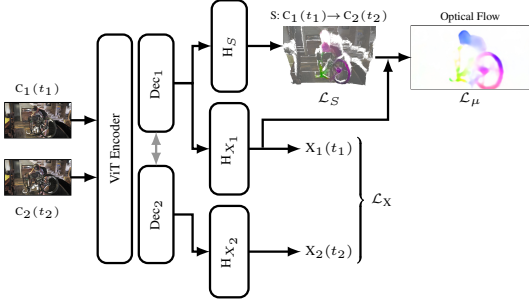


Figure 2. **Overview.** Our method jointly predicts pointmaps (X_1 , X_2) and scene flow S with an information-sharing ViT backbone followed by three prediction heads (H_{X_1} , H_{X_2} , H_S).

zero-shot generalization to in-the-wild scenes.

2.3. Zero-shot Geometry Estimation and Beyond

Deep neural networks pre-trained on large-scale datasets are reshaping AI with their zero-/few-shot adaptability [9, 91]. Their success in language and vision has now extended to 3D applications, with models like DUS3R [102] leveraging large-scale pretraining of cross-view completion [106] to enable a wide range of 3D tasks.

Given a pair of uncalibrated stereo images, DUS3R represents the 3D scene by pointmaps for both images in left camera’s coordinate system with implicit correspondence searching. Later, MAST3R [47] ties DUS3R to metric space and improves on image matching. These large-scale geometry prediction models have empowered a variety of 3D applications, including novel view synthesis [12, 20, 84, 113], surface reconstruction [77], incremental reconstruction [99] and temporal generation [55].

These models are limited to static scenes and cannot reason about motion explicitly. MonST3R [115]—a concurrent work—enhances model robustness when dynamic objects are present. Instead, our method captures the motion field and geometry jointly in 3D with one feedforward pass via a single model that is trained end-to-end.

3. Method

First, we describe the problem with its inputs and outputs, and our approach to joint feedforward scene flow and geometry prediction (Sec. 3.1). Next, we describe our training recipe for in-the-wild generalization (Sec. 3.2), including our scale-adaptive optimization (Sec. 3.3). Finally, we explore the impact of different SF parameterizations (Sec. 3.4).

3.1. Joint, Generalizable Scene Flow Prediction

Problem overview. Given two RGB images $I_1, I_2 \in \mathbb{R}^{H \times W \times 3}$ captured by a single, potentially moving camera over time t , we wish to estimate a 3D mapping that subsumes both 3D camera motion and 3D object motion from

the coordinate frame of the first image C_1 into the coordinate frame of the second image C_2 : $(C_1, t_1) \rightarrow (C_2, t_2)$. We do not have access to camera poses. This mapping could be parameterized in various different ways, such as start and end points, or motion offset vectors [30].

Our method outputs three maps, which combined yield scene flow. The first two, \hat{X}_1 and $\hat{X}_2 \in \mathbb{R}^{H \times W \times 3}$, are pointmaps. They are both represented in the space of camera C_1 , but at times t_1 and t_2 , respectively. Recall that pointmaps are a collection of 3D points \mathbf{x} [102]. The third is a scene flow/offset map $\hat{S} \in \mathbb{R}^{H \times W \times 3}$ expressing the mapping $C_1, t_1 \rightarrow C_2, t_2$.

Pipeline. Accurate scene flow estimation is challenging because it requires understanding the geometry of a scene *and* its motion. We cannot reason about one without considering the other, because after projection to 2D, the two become entangled—and thus scene flow estimation is ill-posed. Moreover, requiring our approach to generalize to unseen domains further complicates the task. We design our pipeline with these observations in mind: First, we use a unified backbone for joint depth and motion prediction. This enables geometry and motion information sharing. Second, we adopt CroCoV2 [106] as our backbone. This enables direct use of pre-trained weights from state-of-the-art geometry prediction models like DUS3R [102] and MAST3R [47] to bootstrap our model’s geometry estimation, which helps improve in-the-wild generalization.

As shown in Fig. 2, our architecture is a ViT [19] model with dual weight-sharing encoder branches (Enc_v), and cross-attended decoders (Dec_v) for each input frame ($v \in \{1, 2\}$). Each decoder comprises B blocks (G_i^v). These are followed by specialized DPT-based [78] heads (H_{X_1} , H_{X_2} , H_S) for pointmap and motion offset prediction:

$$\begin{aligned} \hat{X}_1 &= H_{X_1}(G_0^1, \dots, G_B^1), \\ \hat{X}_2 &= H_{X_2}(G_0^2, \dots, G_B^2), \text{ and} \\ \hat{S} &= H_S(G_0^1, \dots, G_B^1). \end{aligned} \quad (1)$$

Our joint prediction strategy requires a shared internal network representation. As a result, the 3D prior for geometry prediction can help better handle motion, and simultaneously the motion estimation head H_S can help improve geometry prediction through its learned temporal correspondences.

3.2. A Recipe to Create Large-scale Scene Flow Data

If we are to tackle an ill-posed problem with a data-driven approach, we need large and diverse data with high-quality scene flow annotations. However, scene flow is more difficult to measure than other low-level properties like depth and optical flow, as it depends upon both geometry and motion. The resulting scarcity of scene flow datasets has been a major hinderance to the progress of learning-based scene

Table 1. **Training datasets in our recipe.** *OF*: Optical Flow, *SF*: Scene Flow. * For the PointOdyssey dataset, we ignore scenes with smoke.

Dataset	Scene Type		Annotation		Statistics			
	Content	Metric	OF	SF	# Cam	# Frames	# Scenes	$W \times H$
SHIFT [86]	Driving	✓	x	x	6	150k	3000	1280×800
Dynamic Replica [39]	Indoor	✓	✓	x	2	72k	484	1280×720
Virtual KITTI 2 [11]	Driving	✓	✓	✓	2	35k	40	1242×375
MOVi-F [25]	Kubric-style	x	✓	x	1	137k	5736	512×512
PointOdyssey* [120]	Indoor & Kubric-style	✓	x	x	1	100k	39	960×540
Spring [65]	Sintel-style animation	x	✓	✓	2	4k	30	1920×1080

flow prediction methods. Most prior monocular scene flow works [6, 30, 31, 36] train on a specific dataset (*e.g.*, KITTI raw [22]), but each is limited in size and diversity. Some synthetic datasets exist, but these are narrow in their domains. Overall, generalization is restricted by scarce data.

To improve generalization by covering as diverse scene content as possible, we augment four additional dynamic scene datasets for scene flow estimation: SHIFT [86], DynamicReplica [39], MOVi-F [25] and PointOdyssey [120].

With the multiple cameras in the data, the full data recipe (Tab. 1) contains over 1M samples across indoor and outdoor settings, and with real and synthetic dynamic scenarios. This helps to provide accurate and generalizable scene flow prediction.

The data. Each sample consists of data and corresponding annotations for two consecutive timestamps in a video. Specifically, a sample includes two RGB maps, I_1 and I_2 , two depthmaps, D_1 and D_2 , and the corresponding validity maps, M_{D_1} and M_{D_2} , which indicate whether a depth value is available for each pixel in the depthmap. It also includes forward optical flow and validity map, μ and M_μ , as well as forward scene flow and validity map, S and M_S . Finally, each sample provides intrinsics K , relative transformation from C_1 to C_2 , $[R|t]$, and a metric scale indicator $\mathbf{1}_m$ that is ‘1’ if the depth information is metric.

Augmenting datasets for scene flow prediction. Not all datasets provide annotations for scene flow S or optical flow μ . When μ is not provided, we use RAFT [87] to generate pseudo ground truth, and assume that all pixels are valid. When S is not given, we compute pseudo ground truth from the depthmaps, camera poses, and optical flow. To achieve that, we first unproject each pixel \mathbf{p}_1 in I_1 and find the corresponding 3D point

$$\mathbf{x}_1 = \pi^{-1}(D_1[\mathbf{p}_1], K), \quad (2)$$

where $\pi^{-1}(\cdot, \cdot)$ is the inverse of the camera projection operation. Next, we find the corresponding pixel \mathbf{p}_2 to \mathbf{p}_1 via

pixel coordinates \mathbf{p}_1 and optical flow μ and unproject it to produce a second 3D point $\mathbf{x}_2 \in X_2$ in C_2 :

$$\mathbf{p}_2 = \mathbf{p}_1 + \mu[\mathbf{p}_1] \quad (3)$$

$$\mathbf{x}_2 = \pi^{-1}(D_2[\mathbf{p}_2], K). \quad (4)$$

Finally, we can compute the scene flow pseudo ground truth $\mathbf{x}_2 - \mathbf{x}_1$. Note that this uplifting of optical flow and depth to scene flow requires both $\mathbf{p}_1, \mathbf{p}_2$ to have valid depth and for \mathbf{p}_1 to have valid optical flow.

Scene flow is undefined when a 3D point becomes occluded or disoccluded. Even when visibility is not an issue, ground truth data can be in error. To cope with this, we check depth and optical flow validity, as well as occlusion/disocclusion. We follow Meister *et al.* [66] to obtain an occlusion indicator $\mathbf{1}_{\text{cyc}}(\mathbf{p}_1, \mathbf{p}_2)$ through a forward-backward consistency check. Scene flow validity is:

$$M_S[\mathbf{p}_1] = M_\mu[\mathbf{p}_1] \wedge M_{D_1}[\mathbf{p}_1] \wedge M_{D_2}[\mathbf{p}_2] \wedge \mathbf{1}_{\text{cyc}}(\mathbf{p}_1, \mathbf{p}_2). \quad (5)$$

We compute ground truth pointmaps by unprojecting depth maps to camera coordinates. We transform D_2 into C_1 via the relative camera pose:

$$\begin{aligned} X_1 &= \pi^{-1}(D_1, K) \\ X_2 &= [R|t]^{-1}\pi^{-1}(D_2, K). \end{aligned} \quad (6)$$

3.3. Scale-adaptive Optimization

While a large collection of datasets is critical for achieving zero-shot generalization, combining data from diverse datasets, potentially not even designed for our task, is not without cost. One major problem is scale-inconsistency: some data are metric, others are relative (Fig. 3). MiDaS [79] uses diverse dataset for relative depth estimation and introduced a scale-invariant loss to deal with this problem. We propose a similar solution for scene flow that does not require us to give up metric estimation. Instead, we show how to leverage both metric and non-metric data *for metric SF* when properly trained.

Our method’s SF and pointmap outputs are both metric. When $\mathbf{1}_m = 1$, there is nothing to adapt. When $\mathbf{1}_m = 0$, we

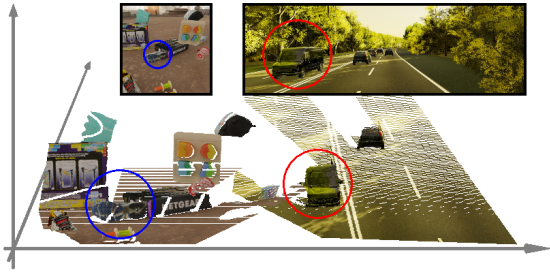


Figure 3. **Different datasets have different scales.** Here we show a frame from MOVi-F [25], which is in relative scale, and one from Virtual KITTI [11], which is in metric units. We need to account for this while training for both geometry and motion.

normalize the ground truth, predicted geometry, and scene flow before computing the loss. Specifically, we compute scale factors for the predicted pointmaps and the ground truth pointmaps separately, as the mean distance from C_1 origin to all valid points:

$$\hat{z} = \frac{\sum_{v \in \{1,2\}} \sum_i M_{D_v}[i] \cdot \|\hat{X}_v[i]\|_2}{\sum_{v \in \{1,2\}} \sum_i M_{D_v}[i]} \quad (7)$$

$$z = \frac{\sum_{v \in \{1,2\}} \sum_i M_{D_v}[i] \cdot \|X_v[i]\|_2}{\sum_{v \in \{1,2\}} \sum_i M_{D_v}[i]}, \quad (8)$$

where $\hat{\cdot}$ indicates predictions. As scene flow and geometry must share a scale, we can use z/\hat{z} to normalize both:

$$\hat{X}_v^* = \hat{X}_v / \hat{z}, \quad \hat{S}^* = \hat{S} / \hat{z} \quad (9)$$

$$X_v^* = X_v / z, \quad S^* = S / z, \quad (10)$$

where $*$ indicates a normalized value. For non-metric data samples, we use normalized pointmaps and scene flow in the loss. Thus, we have a pointmap loss \mathcal{L}_X and a motion offset map loss \mathcal{L}_S :

$$\mathcal{L}_X = \sum_{v \in \{1,2\}} \sum_i M_{D_v}[i] \left(\mathbf{1}_m \|X_v[i] - \hat{X}_v[i]\|_1 + (1 - \mathbf{1}_m) \|X_v^*[i] - \hat{X}_v^*[i]\|_1 \right) \quad (11)$$

$$\mathcal{L}_S = \sum_i M_S[i] \left(\mathbf{1}_m \|S[i] - \hat{S}[i]\|_1 + (1 - \mathbf{1}_m) \|S^*[i] - \hat{S}^*[i]\|_1 \right). \quad (12)$$

Note that we only compute the loss for pixels with valid ground truth.

Optical flow supervision. While our method predicts geometry and motion with a shared encoder-decoder, X and

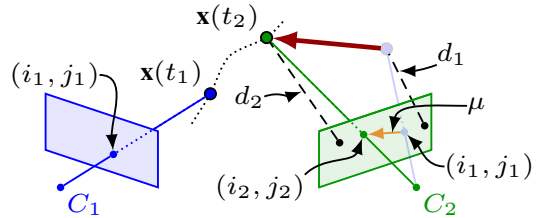


Figure 4. **SF parameterizations.** Given cameras C_1 and C_2 capturing a 3D point at two times, t_1 and t_2 , EP expresses the displacement as the coordinates of $\mathbf{x}(t_2)$ in C_2 , $\Delta D + \text{OF}$ as $d_2 - d_1$ and optical flow μ , and **CSO (ours)** as the 3D offset between the two points, in red in the diagram. Note: The faded blue point to the right has not been transformed from C_1 into C_2 ; it is visualized here with exactly the same numeric coordinates as it has in C_1 .

S are still predicted independently, with no interaction in \mathcal{L}_X nor \mathcal{L}_S . We use optical flow to relate the two in order to improve consistency. The projection of scene flow to optical flow $\hat{\mu}$ relies on X , S , and K , and so a loss over $\hat{\mu}$ encourages the network to produce X and S that are consistent and agree with ground truth intrinsics K during training.

We compute optical flow as the 2D image-space offset between pointmap projections before and after scene flow:

$$\hat{\mu} = \pi(\hat{X}_1 + \hat{S}, K) - \pi(\hat{X}_1, K) \quad (13)$$

$$\mathcal{L}_\mu = \sum_i M_S[i] \|\mu[i] - \hat{\mu}[i]\|_1 \quad (14)$$

Again, we only compute the loss for valid pixels. As optical flow is a projected measure, it is independent of the scaling issue and so no normalization is required.

Final loss. The final optimization target is a weighted mixture of 3D and 2D supervision (Fig. 2):

$$\mathcal{L} = \mathcal{L}_X + \mathcal{L}_S + 0.1\mathcal{L}_\mu \quad (15)$$

3.4. Scene Flow Parameterization Choice

In the literature, scene flow has been parameterized in multiple ways, including as offsets as we have so far discussed [30], but also as end points directly, or as motion-in-depth + optical flow [2, 109], see Fig. 4. We explore the three parameterizations for a generalizable monocular scene flow model. To isolate their contribution to the quality of SF estimation, we define three models. Each variant shares the same network architecture (Sec. 3.1) and only differs in how we interpret the 3-dim output of the scene flow head, H_S .

Camera-space 3D offsets (CSO). This is the parameterization we have discussed thus far, where predicted scene flow \hat{S} parameterizes both camera motion and object motion as a 3D vector field of offsets.

Depth change and optical flow (ΔD +OF). Typical ground truth scene flow annotations are provided as maps of (disparity/depth in C_1 at t_1 , disparity/depth in C_2 at t_2 , optical flow from C_1, t_1 to C_2, t_2). For this parameterization, we assume that optical flow $\hat{\mu}$ is predicted by the first two dimensions of the scene flow head output, and ΔD by the third dimension. To penalize \mathcal{L}_μ , we no longer need to project scene flow as optical flow is predicted directly. But, to penalize \mathcal{L}_S , we need to compose \hat{S} from $\hat{\mu}$, ΔD , \hat{X}_1 , K . First, we add the depth change to the z value of the pointmap \hat{X}_{1z} to obtain the depth after motion in camera space C_2 . Then, for each pixel \mathbf{p} in I_1 , $\hat{\mu}$ tells us which pixel in I_2 it corresponds to. Last, we can compute the 3D position with depth and ray direction, and SF is computed by subtraction:

$$\begin{aligned} D_2 &= \hat{X}_{1z} + \Delta D \\ \hat{S}[\mathbf{p}] &= \pi^{-1}(D_2, K)[\mathbf{p} + \hat{\mu}[\mathbf{p}]] - \hat{X}_1[\mathbf{p}]. \end{aligned} \quad (16)$$

End point (EP). As the pretrained weights from models [47, 102] help the depth estimation side of the problem, and since these models all predict pointmaps instead of offset maps, we can directly use head H_S to predict for I_1 the corresponding 3D point positions in camera space C_2 at t_2 . Then, from H_S 's prediction, \hat{S} , and from H_{X_1} 's prediction, \hat{X}_1 , we can easily compute scene flow as: $\hat{S} - \hat{X}_1$.

4. Experiments

Fig. 1 shows the zero-shot performance of our approach across different scenarios, indoor and outdoor scenes, and over a broad range of scene depths. The animations show interpolation results between the cameras and timestamps of the two input images. They show a different perspective from the input cameras, where both the depth and scene flow are consistent with each other—and correct. We also do extensive quantitative evaluation and ablation studies across several datasets, normalization strategies and training schemes, test zero-shot generalization abilities, as well as the impact of different scene flow parametrizations, all of which we describe in detail in the following sections. However, the key takeaway is much simpler: *The design choices we make in terms of architecture, training recipe, and output parameterization, result in a method that can estimate accurate scene flow in the wild for the first time.*

4.1. Experimental Setting

Datasets. We evaluate our method's scene flow and geometry estimation capabilities on datasets spanning synthetic and real-world scenarios with 3D flow annotations: KITTI Scene Flow [67], Spring [65], and VKITTI2 [11]. Notably, Spring and VKITTI2 currently lack standardized monocular scene flow evaluation protocols. Our evaluation protocol uses only monocular (left camera) sequences (see supplemental material).

Implementation details. We initialize ViT Encoder, Dec_1 , Dec_2 , H_{X_1} and H_{X_2} 's parameters with MAST3R's [47] pretrained weights. If the EP parameterization is used, H_S is also initialized as H_{X_1} .

Comparisons. We compare with methods from two groups. For the first group, SF, we compare with top-performing scene flow estimation methods on the KITTI scene-flow benchmark [67] that have code available. For Self-Mono-SF [30], we use the checkpoint trained on the KITTI Split [23]. We also include OpticalExpansion [109], an algorithm to augment depth estimation models with scene flow prediction function in a generalizable fashion. For OpticalExpansion, we use MAST3R [47] as the depth model, and use the checkpoint trained on *Driving* [63] to prevent leakage of the KITTI test set during training.

For the second group, D +OF (note, different from ΔD +OF which is a scene parameterization), we build baselines by combining depth and optical flow estimation. We first compute the depthmaps for both frames, and then use optical flow and camera intrinsics to estimate scene flow. For depth estimation, we select DUST3R [102], MAST3R [47], and DepthAnythingV2 [111] (metric outdoor version). For optical flow estimation, we use RAFT [87].

Evaluation metrics. We test models on both Monocular Scene Flow Estimation and Depth Estimation. For scene flow evaluation, we follow tradition [26, 59]: End Point Error (EPE), Accuracy Strict (AccS), Accuracy Relax (AccR), and Outliers (Out). For depth estimation, we report both relative depth metrics AbsR-r and δ_{1-r} , and metric depth metrics AbsR-m and δ_{1-m} .

4.2. In/Out-Of-Domain Comparison

We compare under both in-domain and out-of-domain settings on KITTI, VKITTI2 and Spring. The numerical results are summarized in Tab. 2 and visual results are in Fig. 5. Our method achieves superior performance across multiple datasets and metrics quantitatively and qualitatively, demonstrating strong generalization capability.

Comparing with monocular scene flow algorithms. Our method achieves competitive results with previous monocular scene flow algorithms, rows marked with '✓' in Tab. 2, and surpasses them significantly for generalization capabilities. *Ours* outperforms Self-Mono-SF in flow quality even for in-domain evaluations, achieving EPE of 0.452 vs. 0.454 on KITTI, and 0.190 vs. 0.294 on VKITTI2. When evaluating on each dataset, we also train a version of our method that does not use that dataset, listed as *Ours-exclude* in the table, which allows us to evaluate our zero-shot generalization ability. This model significantly outperforms OpticalExpansion in terms of both scene flow and depth estimation on

all datasets. Self-Mono-SF, trained exclusively on KITTI, fails to generalize to the out-of-domain dataset Spring, with AccS degrading from 0.694 on VKITTI2 to 0.251 on Spring and AbsR-r degrading from 0.244 on VKITTI2 to 0.501 on Spring. OpticalExpansion, also trained on autonomous-driving dataset, achieves better results on Spring due to its reliance on an auxiliary robust depth estimation component; however, its EPE on Spring (0.029) still falls short of *Ours-exclude*'s EPE on the same out-of-domain dataset (0.015).

Comparing with $D+OF$ algorithms. Estimating monocular scene flow by simply combining depth and optical flow algorithms leads to poor results. This can be appreciated by comparing the performance of our algorithm (*Ours* in Tab. 2) with $D+OF$ algorithms, which are marked in that table with an 'x'. *Ours* consistently outperforms $D+OF$ algorithms in scene flow quality. Even when our algorithm is used in a zero-shot manner, that is, the dataset used for testing was not seen in training, it performs significantly better than competing $D+OF$ algorithms actually trained on that dataset. For instance, our model tested—but not trained—on KITTI (*Ours-exclude*) achieves an EPE of 0.641, compared with 3.404 by DUST3R and 3.708 by MAST3R when they are finetuned on our data recipe following their original training protocols. This pattern holds across datasets, demonstrating the advantages of our joint approach over separate geometry and motion estimation.

4.3. Scale-Adaptive Optimization

Scale-adaptive optimization is key for our large-scale, diverse data recipe, as we show in Tab. 3 on KITTI dataset.

Scale-handling strategies. The choice significantly impacts both scene flow and geometry estimation. As mentioned in Sec. 3.3, to train across datasets that provide both metric and relative depth, we need to properly handle scale. Here we analyze the impact of four strategies. First, we train our model by simply rescaling our prediction to match the ground truth before computing the loss (*Align* in Tab. 3). Then, we follow DUST3R's strategy, which normalizes the ground truth and our prediction to be between 0 and 1 (*Always* in Tab. 3). We also follow MAST3R's strategy, which assumes the ground truth to be metric and thus does not perform any normalization (*Never* in Tab. 3). Finally, we combine the latter two strategies and normalize the ground truth and our prediction when the ground truth is relative depth and do nothing when it is metric (*Xor* in Tab. 3). The Xor-based variants achieve the best scene flow estimation (EPE: 0.452, 0.501), significantly outperforming *Align* (EPE: 1.596), *Always* (EPE: 0.899), and *Never* (EPE: 0.758). Therefore, we use it as our training strategy.

		KITTI [67] (Real)							
SF Method		Scene Flow Estimation				Depth Estimation			
		EPE↓	AccS↑	AccR↑	Out↓	AbsR-r↓	δ_1 -r↑	AbsR-m↓	δ_1 -m↑
In	✓ <i>Ours</i>	0.452	0.398	0.443	0.873	0.111	0.927	0.236	0.345
	✓ Self-Mono-SF[30]	0.454	0.345	0.435	0.853	0.100	0.905	0.105	0.879
	x DepthAnythingV2[111]	1.835	0.326	0.361	0.931	0.104	0.896	0.134	0.860
	x DUST3R*[102]	3.404	0.268	0.269	0.997	0.129	0.901	0.983	0.000
	x MAST3R*[47]	3.708	0.264	0.267	0.999	0.108	0.929	0.245	0.288
Out	✓ <i>Ours-exclude</i>	0.641	0.392	0.431	0.899	0.116	0.922	0.256	0.237
	✓ OpticalExpansion[109]	2.537	0.348	0.363	0.968	0.132	0.871	0.529	0.172
	x DUST3R[102]	2.088	0.273	0.278	0.986	0.144	0.832	0.968	0.000
	x MAST3R[47]	3.320	0.277	0.280	0.996	0.088	0.921	0.582	0.075
	x MonST3R[115]	3.594	0.269	0.272	0.999	0.099	0.897	0.951	0.000
		VKITTI2 [11] (Synthetic)							
SF Method		Scene Flow Estimation				Depth Estimation			
		EPE↓	AccS↑	AccR↑	Out↓	AbsR-r↓	δ_1 -r↑	AbsR-m↓	δ_1 -m↑
In	✓ <i>Ours</i>	0.190	0.780	0.876	0.484	0.137	0.859	0.236	0.634
	✓ Self-Mono-SF[30]	0.294	0.694	0.751	0.589	0.244	0.568	0.224	0.589
	x DUST3R*[102]	8.822	0.630	0.645	0.910	0.176	0.783	0.981	0.000
	x MAST3R*[47]	5.914	0.635	0.681	0.827	0.138	0.858	0.223	0.672
Out	✓ <i>Ours-exclude</i>	0.409	0.727	0.772	0.696	0.144	0.836	0.168	0.778
	✓ OpticalExpansion[109]	1.809	0.654	0.662	0.946	0.194	0.727	0.203	0.746
	x DUST3R[102]	2.279	0.633	0.673	0.811	0.246	0.586	0.970	0.000
	x MAST3R[47]	2.946	0.666	0.713	0.797	0.166	0.827	0.676	0.050
	x MonST3R[115]	2.206	0.629	0.659	0.853	0.235	0.606	0.949	0.000
		Spring [65] (Synthetic)							
SF Method		Scene Flow Estimation				Depth Estimation			
		EPE↓	AccS↑	AccR↑	Out↓	AbsR-r↓	δ_1 -r↑	AbsR-m↓	δ_1 -m↑
In	✓ <i>Ours</i>	0.013	0.989	0.999	0.813	0.280	0.597	0.679	0.119
	x DUST3R*[102]	0.803	0.242	0.402	0.867	0.324	0.545	0.965	0.000
	x MAST3R*[47]	0.985	0.208	0.267	0.867	0.288	0.550	0.689	0.064
Out	✓ <i>Ours-exclude</i>	0.014	0.992	1.000	0.787	0.294	0.599	0.682	0.130
	✓ Self-Mono-SF[30]	1.005	0.251	0.328	0.880	0.501	0.353	0.784	0.044
	✓ OpticalExpansion[109]	0.029	0.873	0.971	0.805	0.430	0.468	0.804	0.004
	x DepthAnythingV2[111]	0.208	0.496	0.658	0.820	0.379	0.519	0.758	0.181
	x DUST3R[102]	0.275	0.431	0.629	0.831	0.476	0.447	0.939	0.000
x MAST3R[47]	0.610	0.315	0.446	0.855	0.343	0.546	0.811	0.009	

Table 2. **In/Out-of-Domain Quantitative Results: Ours vs. Peers.** We exclude DepthAnythingV2 for VKITTI2 and MonST3R for the Spring dataset as they used the test set for training. *: Finetuned following the original training protocol on our data recipe.

Optical flow supervision. \mathcal{L}_μ improves both scene flow and geometry. Our best model trained without the flow loss \mathcal{L}_μ ('x' in the table) shows a drop of 0.049 in EPE for scene flow. Perhaps surprisingly, using \mathcal{L}_μ also improves depth estimation with an improvement of 0.034 in terms of δ_1 -m.

4.4. Scene Flow Parameterization

We show that zero-shot monocular scene flow estimation is sensitive to parameterization (Sec. 3.4) with an ablation study on the KITTI test set (Tab. 3). CSO achieves superior scene flow accuracy (AccS: 0.398) compared to both EP (AccS: 0.281) and $\Delta D+OF$ (AccS: 0.311) while maintaining comparable depth estimation quality ($\delta_1 - r$: 0.927 vs. 0.927). Notably, $\Delta D+OF$'s performance significantly degrades in scene flow estimation when camera poses are unknown, as evidenced by its poor EPE (11.905) on KITTI. This validates our choice of CSO parameterization for robust scene flow estimation under real-world conditions.

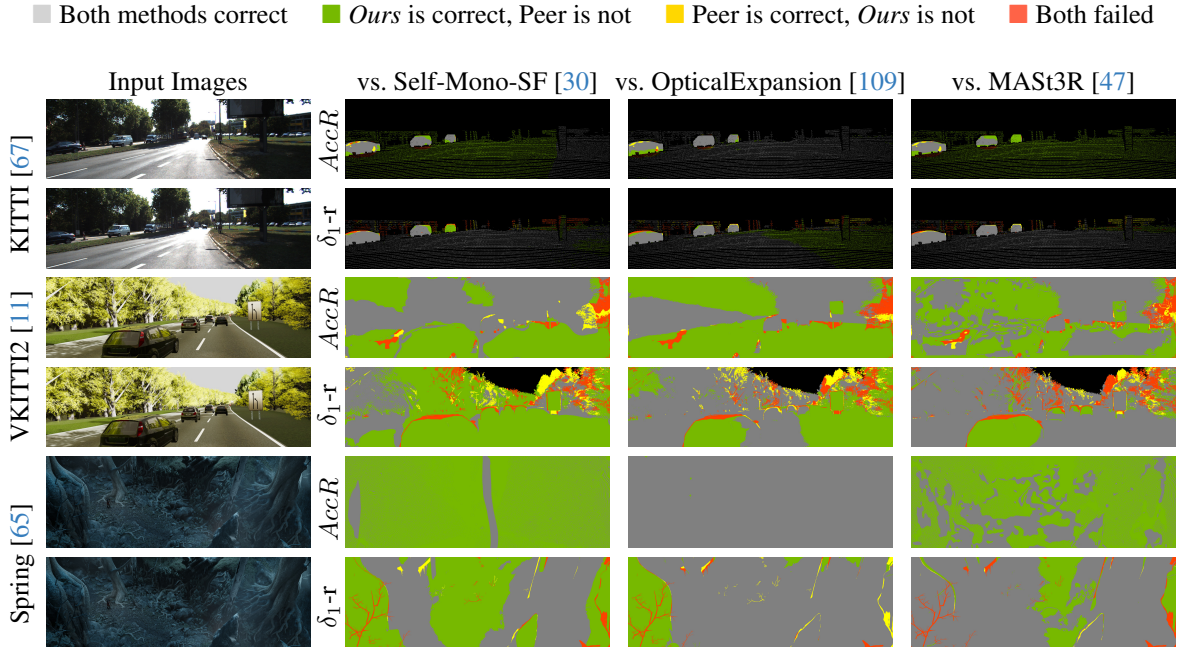


Figure 5. **Qualitative Results: Ours vs. Peers.** We compare our method with the SF peers and one representative of ΔD +OF peers. We show qualitative results from all datasets. For each scene we show a pair of input images, and for each peer we show accuracy maps against *Ours* for both scene flow (*AccR*) and depth (δ_1). Color legend is shown above.

Flow Param.	Loss Design		Scene Flow Estimation				Depth Estimation			
	Norm	\mathcal{L}_μ	EPE \downarrow	AccS \uparrow	AccR \uparrow	Out \downarrow	AbsR-r \downarrow	δ_1 -r \uparrow	AbsR-m \downarrow	δ_1 -m \uparrow
CSO	Align	✓	1.596	0.291	0.295	0.993	0.241	0.620	0.994	0.000
	Always	✓	0.899	0.362	0.384	0.931	0.120	0.915	0.352	0.129
	Never	✓	0.758	0.323	0.359	0.941	0.106	0.930	0.247	0.281
	Xor	x	0.501	0.367	0.410	0.903	0.111	0.927	0.240	0.319
	Xor	✓	0.452	0.398	0.443	0.873	0.111	0.927	0.236	0.345
EP			0.618	0.281	0.362	0.915	0.109	0.926	0.228	0.391
ΔD +OF	Xor	✓	11.905	0.311	0.323	0.993	0.109	0.927	0.231	0.373
CSO			0.452	0.398	0.443	0.873	0.111	0.927	0.236	0.345

Table 3. **Ablate over Scale-Adaptive Optimization and Scene Flow Parameterization on KITTI.** (a) Flow Parameterization (CSO: Camera-space 3D offsets. ΔD +OF: Depth change and optical flow. EP: End Point).

(b) Loss Design \rightarrow Norm: how to handle Dataset Scales with Normalization. \mathcal{L}_μ : whether to use Projected 2D Loss.

4.5. Additional Qualitative Results

We show additional qualitative comparisons for KITTI (Fig. 6) and DAVIS dataset (Fig. 7, 8, 9). Overall, our approach is robust and performs consistently better across different datasets.

5. Conclusion

We present an algorithm for monocular scene flow that jointly estimate geometry and motion in a zero-shot feedforward fashion. Our approach addresses three key challenges

with new contributions: an architecture for joint geometry-motion estimation with a 3D prior, a data recipe to create 1 M diverse training samples from general dynamic datasets and a scale-adaptive optimization to use them, and the careful selection of a scene flow parameterization that uses pointmaps with 3D motion offsets. The resulting model surpasses state-of-the-art methods and baselines built on large-scale models in terms of 3D EPE, and demonstrates strong zero-shot generalization to unseen scenarios from casually-captured videos in DAVIS to robotic manipulation videos in RoboTAP. This generalization ability makes scene flow estimation significantly more practical for real-world applications beyond autonomous driving, like augmented reality and robotics.

Our method, benefiting from 3D prior knowledge learnt for geometry, currently cannot recover from any pitfalls of the pretrained model. Future work should consider using more robust 3D priors to bootstrap our method. Also, camera ego-motion and scene motion are still entangled in our setting; further techniques could be introduced to decompose them and support more downstream applications.

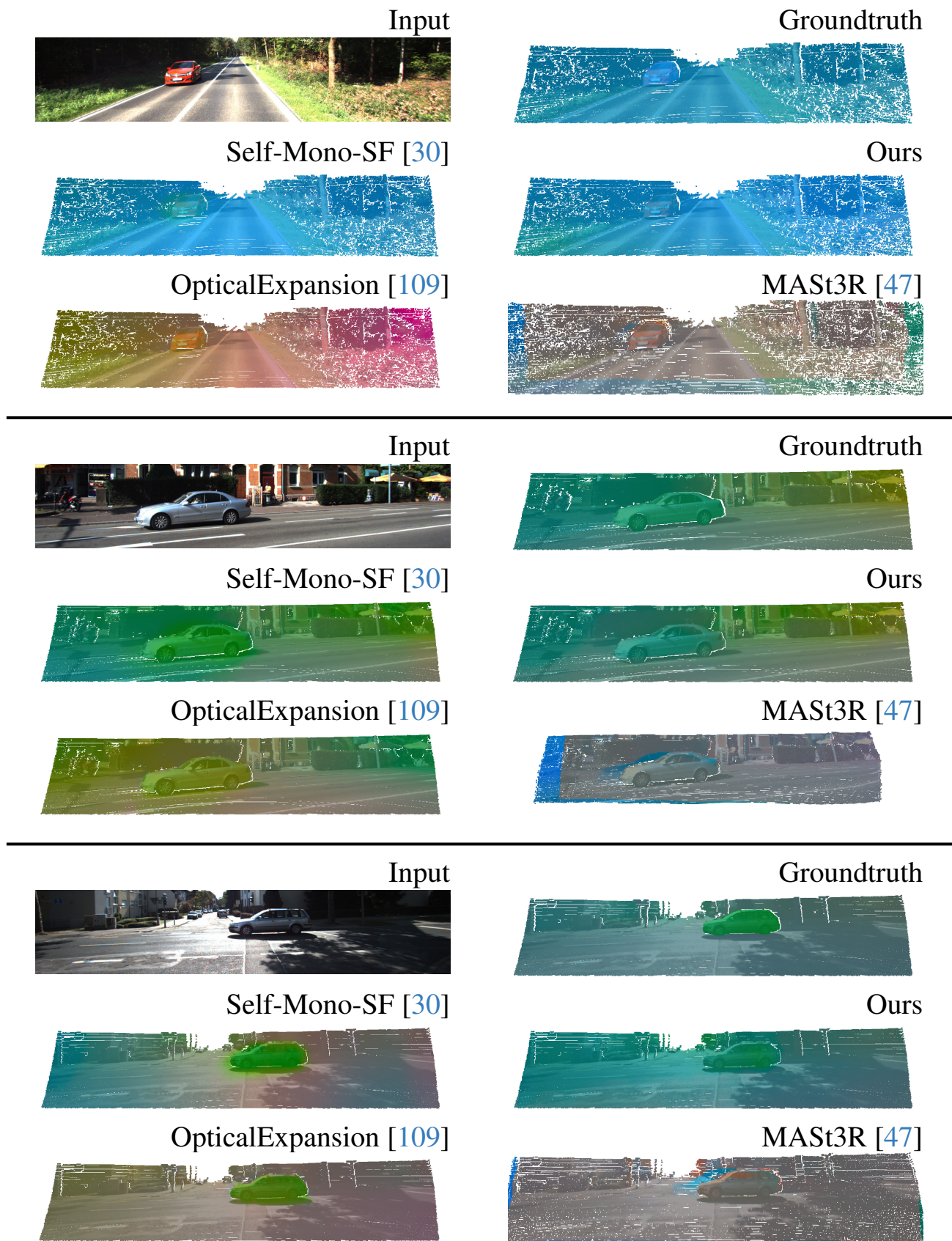


Figure 6. **Additional Qualitative Results on KITTI [67]**, with scene flow represented by CIE-LAB [31] colormap overlaid on corresponding 3D structure estimated for first input image. Ours method shows the highest similarity to the groundtruth.

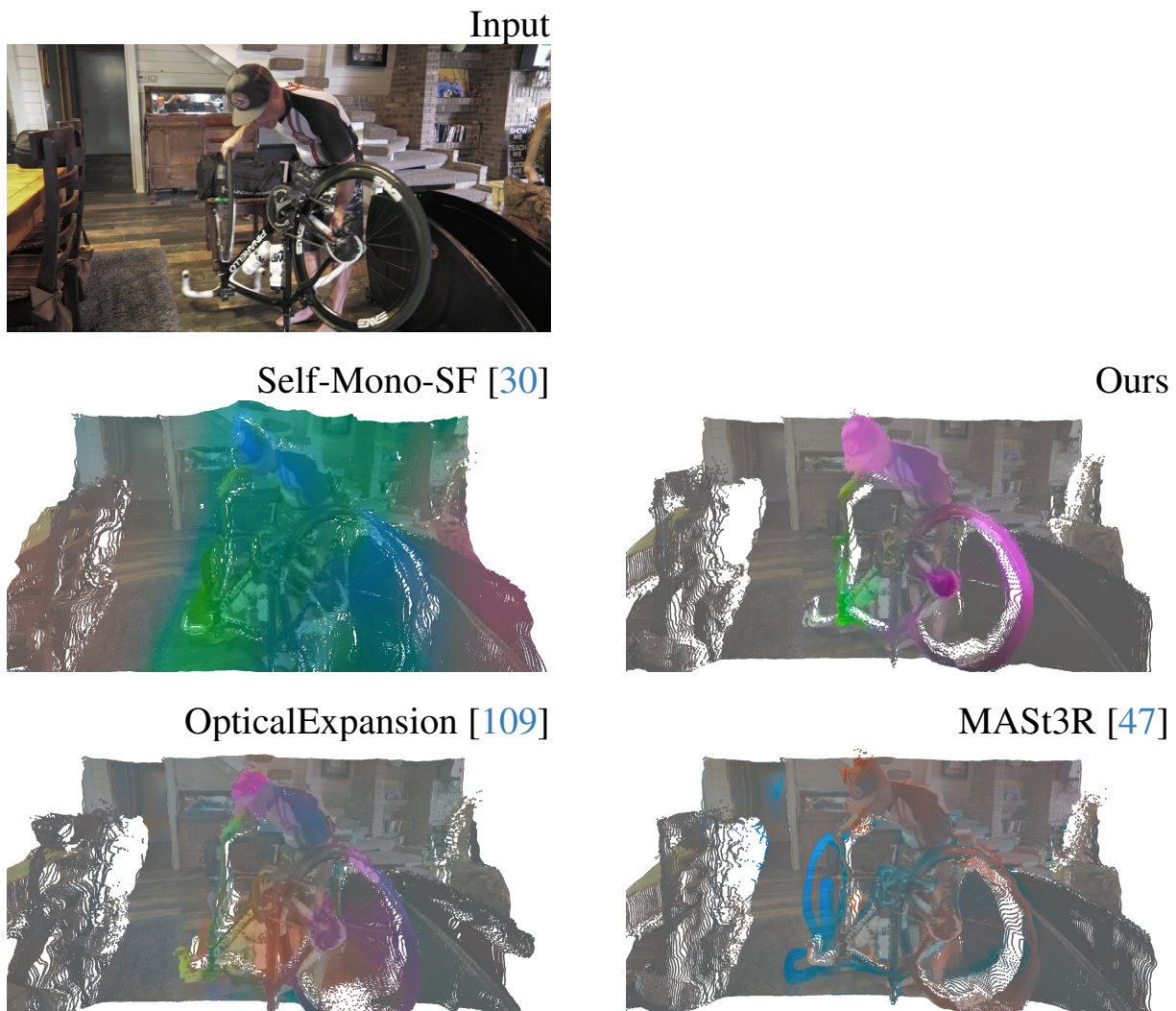


Figure 7. **Additional Qualitative Result on DAVIS [71]**, with scene flow represented by CIE-LAB [31] colormap overlaid on corresponding 3D structure estimated for first input image. Our scene-flow result looks more consistent than other approaches with the bicycle turning motion in this example.



Figure 8. **Additional Qualitative Result on DAVIS [71]**, with scene flow represented by CIE-LAB [31] colormap overlaid on corresponding 3D structure estimated for first input image. As compared to other approaches our approach correctly shows the motion on the legs of the dancer, while identifying most of the background as static.

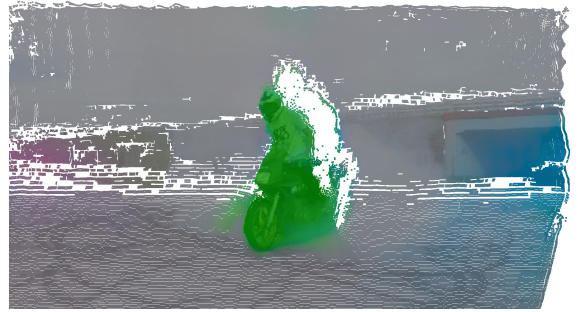
Input



Self-Mono-SF [30]



Ours



OpticalExpansion [109]



MASt3R [47]



Figure 9. **Additional Qualitative Result on DAVIS [71]**, with scene flow represented by CIE-LAB [31] colormap overlaid on corresponding 3D structure estimated for first input image. Our scene-flow result correctly identifies the foreground motion as compared to other approaches.

References

- [1] Rahul Ahuja, Chris Baker, and Wilko Schwarting. Optflow: Fast optimization-based scene flow estimation without supervision. In *IEEE Winter Conference on Applications of Computer Vision (WACV)*, 2024. 2
- [2] Abhishek Badki, Orazio Gallo, Jan Kautz, and Pradeep Sen. Binary ttc: A temporal geofence for autonomous navigation. In *IEEE Conference on Computer Vision and Pattern Recognition (CVPR)*, 2021. 5
- [3] Tali Basha, Yael Moses, and Nahum Kiryati. Multi-view scene flow estimation: A view centered variational approach. In *IEEE Conference on Computer Vision and Pattern Recognition (CVPR)*, 2010. 2
- [4] Ramy Battrawy, René Schuster, and Didier Stricker. Rms-flownet++: Efficient and robust multi-scale scene flow estimation for large-scale point clouds. *International Journal of Computer Vision (IJCV)*, 2024. 2
- [5] Stefan Andreas Baur, David Josef Emmerichs, Frank Moosmann, Peter Pinggera, Björn Ommer, and Andreas Geiger. Slim: Self-supervised lidar scene flow and motion segmentation. In *IEEE International Conference on Computer Vision (ICCV)*, 2021. 2
- [6] Bayram Bayramli, Junhwa Hur, and Hongtao Lu. RAFT-MSF: Self-supervised monocular scene flow using recurrent optimizer. *International Journal of Computer Vision (IJCV)*, 2023. 2, 4
- [7] Aseem Behl, Omid Hosseini Jafari, Siva Karthik Mustikovela, Hassan Abu Alhaija, Carsten Rother, and Andreas Geiger. Bounding boxes, segmentations and object coordinates: How important is recognition for 3d scene flow estimation in autonomous driving scenarios? In *IEEE International Conference on Computer Vision (ICCV)*, 2017. 2
- [8] Aseem Behl, Despoina Paschalidou, Simon Donné, and Andreas Geiger. Pointflownet: Learning representations for rigid motion estimation from point clouds, 2018. 2
- [9] Rishi Bommasani, Drew A. Hudson, Ehsan Adeli, Russ Altman, Simran Arora, Sydney von Arx, Michael S. Bernstein, Jeannette Bohg, Antoine Bosselut, Emma Brunskill, Erik Brynjolfsson, Shyamal Buch, Dallas Card, Rodrigo Castellon, Niladri Chatterji, Annie Chen, Kathleen Creel, Jared Quincy Davis, Dora Demszky, Chris Donahue, Moussa Doumbouya, Esin Durmus, Stefano Ermon, John Etchemendy, Kawin Ethayarajh, Li Fei-Fei, Chelsea Finn, Trevor Gale, Lauren Gillespie, Karan Goel, Noah Goodman, Shelby Grossman, Neel Guha, Tatsunori Hashimoto, Peter Henderson, John Hewitt, Daniel E. Ho, Jenny Hong, Kyle Hsu, Jing Huang, Thomas Icard, Saahil Jain, Dan Jurafsky, Pratyusha Kalluri, Siddharth Karamcheti, Geoff Keeling, Fereshte Khani, Omar Khattab, Pang Wei Koh, Mark Krass, Ranjay Krishna, Rohith Kudithipudi, Ananya Kumar, Faisal Ladhak, Mina Lee, Tony Lee, Jure Leskovec, Isabelle Levent, Xiang Lisa Li, Xuechen Li, Tengyu Ma, Ali Malik, Christopher D. Manning, Suvir Mirchandani, Eric Mitchell, Zanele Munyikwa, Suraj Nair, Avaniika Narayan, Deepak Narayanan, Ben Newman, Allen Nie, Juan Carlos Niebles, Hamed Nilforoshan, Julian Nyarko, Giray Ogut, Laurel Orr, Isabel Papadimitriou, Joon Sung Park, Chris Piech, Eva Portelance, Christopher Potts, Aditi Raghunathan, Rob Reich, Hongyu Ren, Frieda Rong, Yusuf Roohani, Camilo Ruiz, Jack Ryan, Christopher Ré, Dorsa Sadigh, Shiori Sagawa, Keshav Santhanam, Andy Shih, Krishnan Srinivasan, Alex Tamkin, Rohan Taori, Armin W. Thomas, Florian Tramèr, Rose E. Wang, William Wang, Bohan Wu, Jiajun Wu, Yuhuai Wu, Sang Michael Xie, Michihiro Yasunaga, Jiaxuan You, Matei Zaharia, Michael Zhang, Tianyi Zhang, Xikun Zhang, Yuhui Zhang, Lucia Zheng, Kaitlyn Zhou, and Percy Liang. On the opportunities and risks of foundation models, 2022. 1, 3
- [10] Fabian Brickwedde, Steffen Abraham, and Rudolf Mester. Mono-sf: Multi-view geometry meets single-view depth for monocular scene flow estimation of dynamic traffic scenes. In *IEEE International Conference on Computer Vision (ICCV)*, 2019. 2
- [11] Johann Cabon, Naila Murray, and Martin Humenberger. Virtual kitti 2, 2020. 4, 5, 6, 7, 8, 3
- [12] Shan Chen, Jiale Zhou, and Lei Li. Dense point clouds matter: Dust-gs for scene reconstruction from sparse viewpoints, 2024. 3
- [13] Yuhua Chen, Cordelia Schmid, and Cristian Sminchisescu. Self-supervised learning with geometric constraints in monocular video: Connecting flow, depth, and camera. In *IEEE International Conference on Computer Vision (ICCV)*, 2019. 2
- [14] Wencan Cheng and Jong Hwan Ko. Bi-pointflownet: Bidirectional learning for point cloud based scene flow estimation. In *European Conference on Computer Vision (ECCV)*, 2022. 2
- [15] Wencan Cheng and Jong Hwan Ko. Multi-scale bidirectional recurrent network with hybrid correlation for point cloud based scene flow estimation. In *IEEE International Conference on Computer Vision (ICCV)*, 2023.
- [16] David Deng and Avidesh Zakhor. Rsf: Optimizing rigid scene flow from 3d point clouds without labels. In *IEEE Winter Conference on Applications of Computer Vision (WACV)*, 2023. 2
- [17] Lihe Ding, Shaocong Dong, Tingfa Xu, Xinli Xu, Jie Wang, and Jianan Li. Fh-net: A fast hierarchical network for scene flow estimation on real-world point clouds. In *European Conference on Computer Vision (ECCV)*, 2022.
- [18] Guanting Dong, Yueyi Zhang, Hanlin Li, Xiaoyan Sun, and Zhiwei Xiong. Exploiting rigidity constraints for lidar scene flow estimation. In *IEEE Conference on Computer Vision and Pattern Recognition (CVPR)*, 2022. 2
- [19] Alexey Dosovitskiy, Lucas Beyer, Alexander Kolesnikov, Dirk Weissenborn, Xiaohua Zhai, Thomas Unterthiner, Mostafa Dehghani, Matthias Minderer, Georg Heigold, Sylvain Gelly, Jakob Uszkoreit, and Neil Houlsby. An image is worth 16x16 words: Transformers for image recognition at scale. *International Conference on Learning Representations (ICLR)*, 2021. 3
- [20] Zhiwen Fan, Wenyan Cong, Kairun Wen, Kevin Wang, Jian Zhang, Xinghao Ding, Danfei Xu, Boris Ivanovic, Marco Pavone, Georgios Pavlakos, Zhangyang Wang, and Yue

- Wang. Instantsplat: Sparse-view sfm-free gaussian splatting in seconds, 2024. 3
- [21] Andreas Geiger, Philip Lenz, and Raquel Urtasun. Are we ready for autonomous driving? the kitti vision benchmark suite. In *IEEE Conference on Computer Vision and Pattern Recognition (CVPR)*, 2012. 1
- [22] Andreas Geiger, Philip Lenz, Christoph Stiller, and Raquel Urtasun. Vision meets robotics: The kitti dataset. *IJRR*, 2013. 4
- [23] Clement Godard, Oisín Mac Aodha, and Gabriel J. Brostow. Unsupervised monocular depth estimation with left-right consistency. In *IEEE Conference on Computer Vision and Pattern Recognition (CVPR)*, 2017. 6
- [24] Zan Gojcic, Or Litany, Andreas Wieser, Leonidas J. Guibas, and Tolga Birdal. Weakly supervised learning of rigid 3d scene flow, 2021. 2
- [25] Klaus Greff, Francois Belletti, Lucas Beyer, Carl Doersch, Yilun Du, Daniel Duckworth, David J Fleet, Dan Gnanaprasam, Florian Golemo, Charles Herrmann, Thomas Kipf, Abhijit Kundu, Dmitry Lagun, Issam Laradji, Hsueh-Ti (Derek) Liu, Henning Meyer, Yishu Miao, Derek Nowrouzezahrai, Cengiz Oztireli, Etienne Pot, Noha Radwan, Daniel Rebain, Sara Sabour, Mehdi S. M. Sajjadi, Matan Sela, Vincent Sitzmann, Austin Stone, Deqing Sun, Suhani Vora, Ziyu Wang, Tianhao Wu, Kwang Moo Yi, Fangcheng Zhong, and Andrea Tagliasacchi. Kubric: a scalable dataset generator. *IEEE Conference on Computer Vision and Pattern Recognition (CVPR)*, 2022. 4, 5
- [26] Xiuye Gu, Yijie Wang, Chongruo Wu, Yong Jae Lee, and Panqu Wang. Hplflownet: Hierarchical permutohedral lattice flownet for scene flow estimation on large-scale point clouds. In *IEEE Conference on Computer Vision and Pattern Recognition (CVPR)*, 2019. 2, 6
- [27] Simon Hadfield and Richard Bowden. Kinecting the dots: Particle based scene flow from depth sensors. In *IEEE International Conference on Computer Vision (ICCV)*, 2011. 2
- [28] Michael Hornáček, Andrew Fitzgibbon, and Carsten Rother. Spheroflow: 6 dof scene flow from rgb-d pairs. In *IEEE Conference on Computer Vision and Pattern Recognition (CVPR)*, 2014. 2
- [29] Frederic Hugué and Frederic Devernay. A variational method for scene flow estimation from stereo sequences. In *IEEE International Conference on Computer Vision (ICCV)*, 2007. 2
- [30] Junhwa Hur and Stefan Roth. Self-supervised monocular scene flow estimation. In *IEEE Conference on Computer Vision and Pattern Recognition (CVPR)*, 2020. 2, 3, 4, 5, 6, 7, 8, 9, 10, 11, 12
- [31] Junhwa Hur and Stefan Roth. Self-supervised multi-frame monocular scene flow. In *IEEE Conference on Computer Vision and Pattern Recognition (CVPR)*, 2021. 2, 4, 9, 10, 11, 12
- [32] Eddy Ilg, Tonmoy Saikia, Margret Keuper, and Thomas Brox. Occlusions, motion and depth boundaries with a generic network for disparity, optical flow or scene flow estimation. In *European Conference on Computer Vision (ECCV)*, 2018. 2
- [33] Chaokang Jiang, Guangming Wang, Jiuming Liu, Hesheng Wang, Zhuang Ma, Zhenqiang Liu, Zhujin Liang, Yi Shan, and Dalong Du. 3dsflabelling: Boosting 3d scene flow estimation by pseudo auto-labelling. In *IEEE Conference on Computer Vision and Pattern Recognition (CVPR)*, 2024. 2
- [34] Huaizu Jiang, Deqing Sun, Varun Jampani, Zhaoyang Lv, Erik Learned-Miller, and Jan Kautz. Sense: A shared encoder network for scene-flow estimation. In *IEEE International Conference on Computer Vision (ICCV)*, 2019. 2
- [35] Shihao Jiang, Dylan Campbell, Yao Lu, Hongdong Li, and Richard Hartley. Learning to estimate hidden motions with global motion aggregation. In *IEEE International Conference on Computer Vision (ICCV)*, 2021. 2
- [36] Zijie Jiang and Masatoshi Okutomi. Emr-msf: Self-supervised recurrent monocular scene flow exploiting ego-motion rigidity. In *IEEE International Conference on Computer Vision (ICCV)*, 2023. 2, 4
- [37] Yang Jiao, Trac D. Tran, and Guangming Shi. Effiscene: Efficient per-pixel rigidity inference for unsupervised joint learning of optical flow, depth, camera pose and motion segmentation. In *IEEE Conference on Computer Vision and Pattern Recognition (CVPR)*, 2021. 2
- [38] Philipp Jund, Chris Sweeney, Nichola Abdo, Zhifeng Chen, and Jonathon Shlens. Scalable scene flow from point clouds in the real world. *Robotics and Automation Letters (RA-L)*, 2022. 2
- [39] Nikita Karaev, Ignacio Rocco, Benjamin Graham, Natalia Neverova, Andrea Vedaldi, and Christian Rupprecht. Dynamicstereo: Consistent dynamic depth from stereo videos. *IEEE Conference on Computer Vision and Pattern Recognition (CVPR)*, 2023. 4
- [40] Ishan Khatri, Kyle Vedder, Neehar Peri, Deva Ramanan, and James Hays. I Can't Believe It's Not Scene Flow! In *European Conference on Computer Vision (ECCV)*, 2024. 2
- [41] Alexander Kirillov, Eric Mintun, Nikhila Ravi, Hanzi Mao, Chloe Rolland, Laura Gustafson, Tete Xiao, Spencer Whitehead, Alexander C. Berg, Wan-Yen Lo, et al. Segment anything. In *IEEE Conference on Computer Vision and Pattern Recognition (CVPR)*, 2023. 1
- [42] Yair Kittenplon, Yonina C. Eldar, and Dan Raviv. Flow-step3d: Model unrolling for self-supervised scene flow estimation. In *IEEE Conference on Computer Vision and Pattern Recognition (CVPR)*, 2021. 2
- [43] Georg S. W. Klein and David William Murray. Parallel tracking and mapping for small ar workspaces. *IEEE and ACM International Symposium on Mixed and Augmented Reality (ISMAR)*, 2007. 1
- [44] Hsueh-Ying Lai, Yi-Hsuan Tsai, and Wei-Chen Chiu. Bridging stereo matching and optical flow via spatiotemporal correspondence. In *IEEE Conference on Computer Vision and Pattern Recognition (CVPR)*, 2019. 2
- [45] Itai Lang, Dror Aiger, Forrester Cole, Shai Avidan, and Michael Rubinstein. SCOOP: Self-Supervised Correspondence and Optimization-Based Scene Flow. In *IEEE Conference on Computer Vision and Pattern Recognition (CVPR)*, 2023. 2
- [46] Seokju Lee, Sunghoon Im, Stephen Lin, and In So Kweon. Learning residual flow as dynamic motion from stereo

- videos. In *International Conference on Intelligent Robots and Systems (IROS)*, 2019. 2
- [47] Vincent Leroy, Yohann Cabon, and Jerome Revaud. Grounding image matching in 3d with mast3r, 2024. 1, 2, 3, 6, 7, 8, 9, 10, 11, 12
- [48] Ruibo Li, Guosheng Lin, Tong He, Fayao Liu, and Chunhua Shen. Hcrf-flow: Scene flow from point clouds with continuous high-order crfs and position-aware flow embedding. In *IEEE Conference on Computer Vision and Pattern Recognition (CVPR)*, 2021. 2
- [49] Ruibo Li, Guosheng Lin, and Lihua Xie. Self-point-flow: Self-supervised scene flow estimation from point clouds with optimal transport and random walk. In *IEEE Conference on Computer Vision and Pattern Recognition (CVPR)*, 2021.
- [50] Ruibo Li, Chi Zhang, Guosheng Lin, Zhe Wang, and Chunhua Shen. Rigidflow: Self-supervised scene flow learning on point clouds by local rigidity prior. In *IEEE Conference on Computer Vision and Pattern Recognition (CVPR)*, 2022.
- [51] Xueqian Li, Jhony Kaesemodel Pontes, and Simon Lucey. Neural scene flow prior. *Advances in Neural Information Processing Systems (NeurIPS)*, 2021. 2
- [52] Xueqian Li, Jianqiao Zheng, Francesco Ferroni, Jhony Kaesemodel Pontes, and Simon Lucey. Fast neural scene flow. In *IEEE International Conference on Computer Vision (ICCV)*, 2023. 2
- [53] Yangyan Li, Rui Bu, Mingchao Sun, Wei Wu, Xinhan Di, and Baoquan Chen. Pointnet: Convolution on x-transformed points. In *Advances in Neural Information Processing Systems (NeurIPS)*, 2018. 2
- [54] Han Ling, Yinghui Sun, Quansen Sun, and Zhenwen Ren. Learning optical expansion from scale matching. In *IEEE Conference on Computer Vision and Pattern Recognition (CVPR)*, 2023. 2
- [55] Fangfu Liu, Wenqiang Sun, Hanyang Wang, Yikai Wang, Haowen Sun, Junliang Ye, Jun Zhang, and Yueqi Duan. Reconx: Reconstruct any scene from sparse views with video diffusion model, 2024. 3
- [56] Haisong Liu, Tao Lu, Yihui Xu, Jia Liu, Wenjie Li, and Lijun Chen. Camliflow: bidirectional camera-lidar fusion for joint optical flow and scene flow estimation. In *IEEE Conference on Computer Vision and Pattern Recognition (CVPR)*, 2022. 2
- [57] Jiuming Liu, Guangming Wang, Weicai Ye, Chaokang Jiang, Jinru Han, Zhe Liu, Guofeng Zhang, Dalong Du, and Hesheng Wang. Diffflow3d: Toward robust uncertainty-aware scene flow estimation with iterative diffusion-based refinement. In *IEEE Conference on Computer Vision and Pattern Recognition (CVPR)*, 2024. 2
- [58] Liang Liu, Guangyao Zhai, Wenlong Ye, and Yong Liu. Unsupervised learning of scene flow estimation fusing with local rigidity. In *International Joint Conference on Artificial Intelligence (IJCAI)*, 2019. 2
- [59] Xingyu Liu, Charles R Qi, and Leonidas J Guibas. FlowNet3d: Learning scene flow in 3d point clouds. *IEEE Conference on Computer Vision and Pattern Recognition (CVPR)*, 2019. 2, 6
- [60] Chenxu Luo, Zhenheng Yang, Peng Wang, Yang Wang, Wei Xu, Ram Nevatia, and Alan Yuille. Every pixel counts ++: Joint learning of geometry and motion with 3d holistic understanding. *IEEE Transactions on Pattern Analysis and Machine Intelligence (TPAMI)*, 2020. 2
- [61] Zhaoyang Lv, Kihwan Kim, Alejandro Troccoli, Deqing Sun, James Rehg, and Jan Kautz. Learning rigidity in dynamic scenes with a moving camera for 3d motion field estimation. In *European Conference on Computer Vision (ECCV)*, 2018. 2
- [62] Wei-Chiu Ma, Shenlong Wang, Rui Hu, Yuwen Xiong, and Raquel Urtasun. Deep rigid instance scene flow. In *IEEE Conference on Computer Vision and Pattern Recognition (CVPR)*, 2019. 2
- [63] Nikolaus Mayer, Eddy Ilg, Philip Hausser, Philipp Fischer, Daniel Cremers, Alexey Dosovitskiy, and Thomas Brox. A large dataset to train convolutional networks for disparity, optical flow, and scene flow estimation. In *IEEE Conference on Computer Vision and Pattern Recognition (CVPR)*, 2016. 2, 6, 4
- [64] Lukas Mehl, Azin Jahedi, Jenny Schmalfluss, and Andrés Bruhn. M-FUSE: Multi-frame fusion for scene flow estimation. In *IEEE Winter Conference on Applications of Computer Vision (WACV)*, 2023. 2
- [65] Lukas Mehl, Jenny Schmalfluss, Azin Jahedi, Yaroslava Nalivayko, and Andrés Bruhn. Spring: A high-resolution high-detail dataset and benchmark for scene flow, optical flow and stereo. In *IEEE Conference on Computer Vision and Pattern Recognition (CVPR)*, 2023. 4, 6, 7, 8, 3
- [66] Simon Meister, Junhwa Hur, and Stefan Roth. UnFlow: Unsupervised learning of optical flow with a bidirectional census loss. In *AAAI Conference on Artificial Intelligence (AAAI)*, New Orleans, Louisiana, 2018. 4
- [67] Moritz Menze and Andreas Geiger. Object scene flow for autonomous vehicles. *IEEE Conference on Computer Vision and Pattern Recognition (CVPR)*, 2015. 2, 6, 7, 8, 9, 3, 4
- [68] Himangi Mittal, Brian Okorn, and David Held. Just go with the flow: Self-supervised scene flow estimation. In *IEEE Conference on Computer Vision and Pattern Recognition (CVPR)*, 2020. 2
- [69] Bojun Ouyang and Dan Raviv. Occlusion guided scene flow estimation on 3d point clouds. In *IEEE Conference on Computer Vision and Pattern Recognition (CVPR)*, 2021.
- [70] Chensheng Peng, Guangming Wang, Xian Wan Lo, Xinrui Wu, Chenfeng Xu, Masayoshi Tomizuka, Wei Zhan, and Hesheng Wang. Delflow: Dense efficient learning of scene flow for large-scale point clouds. In *IEEE International Conference on Computer Vision (ICCV)*, 2023. 2
- [71] F. Perazzi, J. Pont-Tuset, B. McWilliams, L. Van Gool, M. Gross, and A. Sorkine-Hornung. A benchmark dataset and evaluation methodology for video object segmentation. In *IEEE Conference on Computer Vision and Pattern Recognition (CVPR)*, 2016. 10, 11, 12
- [72] Jean-Philippe Pons, Renaud Keriven, and Olivier Faugeras. Multi-view stereo reconstruction and scene flow estimation with a global image-based matching score. *International Journal of Computer Vision (IJCV)*, 2007. 2
- [73] Jhony Kaesemodel Pontes, James Hays, and Simon Lucey. Scene flow from point clouds with or without learning. In *International Conference on 3D Vision (3DV)*, 2020. 2

- [74] Gilles Puy, Alexandre Boulch, and Renaud Marlet. FLOT: Scene Flow on Point Clouds Guided by Optimal Transport. In *European Conference on Computer Vision (ECCV)*, 2020. 2
- [75] Yi-Ling Qiao, Lin Gao, Yu-Kun Lai, Fang-Lue Zhang, Ming-Ze Yuan, and Shihong Xia. Sf-net: Learning scene flow from rgb-d images with cnns. In *British Machine Vision Conference (BMVC)*, 2018. 2
- [76] Julian Quiroga, Thomas Brox, Frédéric Devernay, and James Crowley. Dense semi-rigid scene flow estimation from rgb-d images. In *European Conference on Computer Vision (ECCV)*, Cham, 2014. 2
- [77] Kevin Raj, Christopher Wewer, Raza Yunus, Eddy Ilg, and Jan Eric Lenssen. Spurfies: Sparse surface reconstruction using local geometry priors, 2024. 3
- [78] Rene Ranftl, Alexey Bochkovskiy, and Vladlen Koltun. Vision transformers for dense prediction. In *IEEE International Conference on Computer Vision (ICCV)*, 2021. 3
- [79] René Ranftl, Katrin Lasinger, David Hafner, Konrad Schindler, and Vladlen Koltun. Towards robust monocular depth estimation: Mixing datasets for zero-shot cross-dataset transfer. *IEEE Transactions on Pattern Analysis and Machine Intelligence (TPAMI)*, 2022. 2, 4
- [80] Anurag Ranjan, Varun Jampani, Lukas Balles, Kihwan Kim, Deqing Sun, Jonas Wulff, and Michael J. Black. Competitive collaboration: Joint unsupervised learning of depth, camera motion, optical flow and motion segmentation. In *IEEE Conference on Computer Vision and Pattern Recognition (CVPR)*, 2019. 2
- [81] Zhile Ren, Deqing Sun, Jan Kautz, and Erik Sudderth. Cascaded scene flow prediction using semantic segmentation. In *International Conference on 3D Vision (3DV)*, 2017. 2
- [82] Rohan Saxena, René Schuster, Oliver Wasenmuller, and Didier Stricker. Pwoc-3d: Deep occlusion-aware end-to-end scene flow estimation. In *IEEE Intelligent Vehicles Symposium (IV)*, 2019.
- [83] Rene Schuster, Oliver Wasenmuller, Georg Kuschik, Christian Bailer, and Didier Stricker. Sceneflowfields: Dense interpolation of sparse scene flow correspondences. In *IEEE Winter Conference on Applications of Computer Vision (WACV)*, 2018. 2
- [84] Brandon Smart, Chuanxia Zheng, Iro Laina, and Victor Adrian Prisacariu. Splatt3r: Zero-shot gaussian splatting from uncalibrated image pairs, 2024. 3
- [85] Xiuchao Sui, Shaohua Li, Xue Geng, Yan Wu, Xinxing Xu, Yong Liu, Rick Goh, and Hongyuan Zhu. Craft: Cross-attentional flow transformer for robust optical flow. In *IEEE Conference on Computer Vision and Pattern Recognition (CVPR)*, 2022. 2
- [86] Tao Sun, Mattia Segu, Janis Postels, Yuxuan Wang, Luc Van Gool, Bernt Schiele, Federico Tombari, and Fisher Yu. SHIFT: a synthetic driving dataset for continuous multi-task domain adaptation. In *IEEE Conference on Computer Vision and Pattern Recognition (CVPR)*, 2022. 4
- [87] Zachary Teed and Jia Deng. Raft: Recurrent all-pairs field transforms for optical flow. In *European Conference on Computer Vision (ECCV)*, 2020. 4, 6
- [88] Zachary Teed and Jia Deng. Raft-3d: Scene flow using rigid-motion embeddings. In *IEEE Conference on Computer Vision and Pattern Recognition (CVPR)*, 2021. 2
- [89] Ravi Kumar Thakur and Snehasis Mukherjee. Scenednet: A deep learning approach for scene flow estimation. In *International Conference on Control, Automation, Robotics and Vision (ICARCV)*, 2018. 2
- [90] Ivan Tishchenko, Sandro Lombardi, Martin R Oswald, and Marc Pollefeys. Self-supervised learning of non-rigid residual flow and ego-motion. In *International Conference on 3D Vision (3DV)*, 2020. 2
- [91] Hugo Touvron, Thibaut Lavril, Gautier Izacard, Xavier Martinet, Marie-Anne Lachaux, Timothée Lacroix, Baptiste Rozière, Naman Goyal, Eric Hambro, Faisal Azhar, Aurelien Rodriguez, Armand Joulin, Edouard Grave, and Guillaume Lample. Llama: Open and efficient foundation language models, 2023. 3
- [92] Kyle Vedder, Neehar Peri, Nathaniel Chodosh, Ishan Khatri, Eric Eaton, Dinesh Jayaraman, Yang Liu Deva Ramanan, and James Hays. ZeroFlow: Fast Zero Label Scene Flow via Distillation. *International Conference on Learning Representations (ICLR)*, 2024. 2
- [93] S. Vedula, P. Rander, R. Collins, and T. Kanade. Three-dimensional scene flow. *IEEE Transactions on Pattern Analysis and Machine Intelligence (TPAMI)*, 2005. 2
- [94] Christoph Vogel, Konrad Schindler, and Stefan Roth. 3d scene flow estimation with a rigid motion prior. In *IEEE International Conference on Computer Vision (ICCV)*, 2011.
- [95] Christoph Vogel, Konrad Schindler, and Stefan Roth. Piecewise rigid scene flow. In *IEEE International Conference on Computer Vision (ICCV)*, 2013.
- [96] Christoph Vogel, Stefan Roth, and Konrad Schindler. View-consistent 3d scene flow estimation over multiple frames. In *European Conference on Computer Vision (ECCV)*, 2014.
- [97] Christoph Vogel, Konrad Schindler, and Stefan Roth. 3d scene flow estimation with a piecewise rigid scene model. *International Journal of Computer Vision (IJCV)*, 2015. 2
- [98] Guangming Wang, Yunzhe Hu, Zhe Liu, Yiyang Zhou, Masayoshi Tomizuka, Wei Zhan, and Hesheng Wang. What matters for 3d scene flow network. In *European Conference on Computer Vision (ECCV)*, 2022. 2
- [99] Hengyi Wang and Lourdes Agapito. 3d reconstruction with spatial memory, 2024. 3
- [100] Haiyan Wang, Jiahao Pang, Muhammad A Lodhi, Yingli Tian, and Dong Tian. Festa: Flow estimation via spatial-temporal attention for scene point clouds. In *IEEE Conference on Computer Vision and Pattern Recognition (CVPR)*, 2021. 2
- [101] Jun Wang, Xiaolong Li, Alan Sullivan, Lynn Abbott, and Siheng Chen. Pointmotionnet: Point-wise motion learning for large-scale lidar point clouds sequences. In *IEEE Conference on Computer Vision and Pattern Recognition Workshops (CVPRW)*, 2022. 2
- [102] Shuzhe Wang, Vincent Leroy, Yohann Cabon, Boris Chidlovskii, and Jerome Revaud. Dust3r: Geometric 3d vision made easy. In *IEEE Conference on Computer Vision and Pattern Recognition (CVPR)*, 2024. 1, 2, 3, 6, 7

- [103] Yang Wang, Peng Wang, Zhenheng Yang, Chenxu Luo, Yi Yang, and Wei Xu. Unos: Unified unsupervised optical-flow and stereo-depth estimation by watching videos. In *IEEE Conference on Computer Vision and Pattern Recognition (CVPR)*, 2019. 2
- [104] A. Wedel, T. Brox, T. Vaudrey, C. Rabe, U. Franke, and D. Cremers. Stereoscopic scene flow computation for 3d motion understanding. *International Journal of Computer Vision (IJCV)*, 2011. 2
- [105] Yi Wei, Ziyi Wang, Yongming Rao, Jiwen Lu, and Jie Zhou. PV-RAFT: Point-Voxel Correlation Fields for Scene Flow Estimation of Point Clouds. In *IEEE Conference on Computer Vision and Pattern Recognition (CVPR)*, 2021. 2
- [106] Philippe Weinzaepfel, Thomas Lucas, Vincent Leroy, Yohann Cabon, Vaibhav Arora, Romain Brégier, Gabriela Csurka, Leonid Antsfeld, Boris Chidlovskii, and Jérôme Revaud. CroCo v2: Improved Cross-view Completion Pre-training for Stereo Matching and Optical Flow. In *IEEE International Conference on Computer Vision (ICCV)*, 2023. 3
- [107] Wenxuan Wu, Zhi Yuan Wang, Zhuwen Li, Wei Liu, and Li Fuxin. Pointpwc-net: A coarse-to-fine network for supervised and self-supervised scene flow estimation on 3d point clouds. In *European Conference on Computer Vision (ECCV)*, 2020. 2
- [108] Mengda Xu, Zhenjia Xu, Yinghao Xu, Cheng Chi, Gordon Wetzstein, Manuela Veloso, and Shuran Song. Flow as the cross-domain manipulation interface. In *Conference on Robot Learning (CoRL)*, 2024. 1
- [109] Gengshan Yang and Deva Ramanan. Upgrading optical flow to 3d scene flow through optical expansion. In *IEEE Conference on Computer Vision and Pattern Recognition (CVPR)*, 2020. 2, 5, 6, 7, 8, 9, 10, 11, 12, 4
- [110] Lihe Yang, Bingyi Kang, Zilong Huang, Xiaogang Xu, Jiashi Feng, and Hengshuang Zhao. Depth anything: Unleashing the power of large-scale unlabeled data. In *IEEE Conference on Computer Vision and Pattern Recognition (CVPR)*, 2024. 1
- [111] Lihe Yang, Bingyi Kang, Zilong Huang, Zhen Zhao, Xiaogang Xu, Jiashi Feng, and Hengshuang Zhao. Depth anything v2. In *Advances in Neural Information Processing Systems (NeurIPS)*, 2024. 1, 6, 7
- [112] Zhichao Yin and Jianping Shi. Geonet: Unsupervised learning of dense depth, optical flow and camera pose. In *IEEE Conference on Computer Vision and Pattern Recognition (CVPR)*, 2018. 2
- [113] Hanyang Yu, Xiaoxiao Long, and Ping Tan. Lm-gaussian: Boost sparse-view 3d gaussian splatting with large model priors, 2024. 3
- [114] Feihu Zhang, Oliver J. Woodford, Victor Adrian Prisacariu, and Philip H.S. Torr. Separable flow: Learning motion cost volumes for optical flow estimation. In *IEEE International Conference on Computer Vision (ICCV)*, 2021. 2
- [115] Junyi Zhang, Charles Herrmann, Junhwa Hur, Varun Jampani, Trevor Darrell, Forrester Cole, Deqing Sun, and Ming-Hsuan Yang. Monst3r: A simple approach for estimating geometry in the presence of motion, 2024. 3, 7
- [116] Qingwen Zhang, Yi Yang, Peizheng Li, Olov Andersson, and Patric Jensfelt. SeFlow: A self-supervised scene flow method in autonomous driving. In *European Conference on Computer Vision (ECCV)*, 2024. 2
- [117] Ye Zhang and C. Kambhampettu. On 3d scene flow and structure estimation. In *IEEE Conference on Computer Vision and Pattern Recognition (CVPR)*, 2001. 2
- [118] Yushan Zhang, Johan Edstedt, Bastian Wandt, Per-Erik Forssen, Maria Magnusson, and Michael Felsberg. GMSF: Global matching scene flow. In *Advances in Neural Information Processing Systems (NeurIPS)*, 2023. 2
- [119] Yushan Zhang, Bastian Wandt, Maria Magnusson, and Michael Felsberg. Diffsf: Diffusion models for scene flow estimation. *arXiv preprint arXiv:2403.05327*, 2024. 2
- [120] Yang Zheng, Adam W. Harley, Bokui Shen, Gordon Wetzstein, and Leonidas J. Guibas. Pointodyssey: A large-scale synthetic dataset for long-term point tracking. In *IEEE International Conference on Computer Vision (ICCV)*, 2023. 4
- [121] Y. Zhou, G. Mei, Y. Wang, F. Poiesi, and Y. Wan. Attentive Multimodal Fusion for Optical and Scene Flow. *Robotics and Automation Letters (RA-L)*, 2023. 2
- [122] Yuliang Zou, Zelun Luo, and Jia-Bin Huang. Df-net: Un-supervised joint learning of depth and flow using cross-task consistency. In *European Conference on Computer Vision (ECCV)*, 2018. 2

Zero-Shot Monocular Scene Flow Estimation in the Wild

Supplementary Material

In this supplementary material, we present additional technical details and evaluations pertaining to our model architecture, dataset, and methodology. Please check our supplementary video for a high-level overview and abundant qualitative results with comparisons.

A. Additional Experimental Setting

Datasets. For evaluation on the Spring Dataset, we use a subset of the training set {0005, 0009, 0013, 0017, 0023, 0037, 0044}. For VKITTI2, we designate Scene18 as the test sequence due to its overlap with KITTI Scene Flow training data, preventing data contamination. VKITTI2 is created to reproduce several scenes of KITTI, thus we consider methods trained on VKITTI2 to be in-domain with KITTI experiments.

Implementation Details. All experiments are trained with 8 NVIDIA A100 GPUs for 50 epochs, which take 12 hours. We accumulate gradients every 2 steps, and clip gradients by norm value 0.5. We have 8 DDP processes with a batch size of 4, thus our effective batch size is $4 \times 8 \times 2 = 64$.

We select a learning rate of $1e^{-6}$ for the encoder-decoder, $1e^{-6}$ for the pointmap heads, and $1e^{-4}$ for the offset heads. For the first 8 epochs, all learning rates start from 0.1 of above values, and gradually warm up. Note that, differently from DUST3R [102] or MAST3R [47], our heads do not predict confidence maps as we found empirically that they made our training unstable.

Training Datasets. At each epoch, we re-sample $1e^4$ examples from the whole Data Recipe for training by balancing different datasets considering diversity and statistics (Tab. 5). 10000 samples for each epoch is made of: (SHIFT:2024, DynamicReplica:1942, VKITTI2:958, MOVIF:3560, PointOdyssey:1400, Spring:116). We resize and crop all dataset samples into 288×512 resolution. For stereo cameras, we ignore right camera frames.

Resolution/Scale Alignment. During evaluation, we resize inputs to be width-512 and resize outputs later. If scale alignment is required, we compute median scale between the predicted and ground-truth pointmap following DUST3R [102], and scale both the pointmap and sceneflow.

Baselines. DUST3R/MASt3R predict a pointmap for the second frame in the first frame’s coordinate system. However, for scene flow, we need geometry for the second frame in the second frame’s coordinate system. As such, for the Spring and VKITTI2 datasets, we use the ground truth camera pose to transform the pointmaps into the second frame’s

coordinate system such that we can create depth maps for the second frame. For KITTI, we use DUST3R’s [102] pose estimation method to infer camera pose.

Resolution/Scale Alignment. For fairness, most methods resize inputs to be width-512 during inference. Self-Mono-SF requires 256×832 , while OpticalExpansion [109] requires 384×1280 . For DUST3R / MAST3R, we multiply pointmaps by estimating scaling factor. For Self-Mono-SF and DepthAnythingV2-metric, the scale factor is computed for each depth estimation/groundtruth pair.

Evaluation Metrics.

EPE: $\|\widehat{sf} - sf\|_2$ averaged over each pixel, where, \widehat{sf} and sf denote the estimated and ground truth scene flows respectively.

AccS: Percentage of points where $EPE < 0.05$ or relative error $< 5\%$.

AccR: Percentage of points where $EPE < 0.1$ or relative error $< 10\%$.

Out: Percentage of points where $EPE > 0.3$ or relative error $> 10\%$.

AbsRel: Absolute relative error $|d^* - d|/d$.

δ_1 : Percentage of $\max(d^*/d, d/d^*) < 1.25$.

B. Additional experiments

B.1. Does Joint Estimation Help?

Key to our method’s success is our design that forces the model to predict geometry and scene flow jointly. To validate this statement we present an ablation study in Tab. 4, which shows different pretraining strategies.

Our analysis allows us to make a few observations. First, we compare the performance of our method when we train the offset head from scratch, and when we initialize it with either DUST3R or MAST3R’s pretrained model. Initializing the offset head results in significantly lower (better) EPE and AbsR-r numbers in Tab. 4. From them, the importance of high-quality 3D priors for the offset head is therefore clear, which also confirms the entanglement of depth and motion predictions. Second, our approach outperforms the combination of MAST3R, a state-of-the-art depth estimation algorithm, and RAFT, a state-of-the-art optical flow algorithm—and the algorithm we use to generate the pseudo ground truth we train on. Our approach combining MAST3R prior with the offset head achieves optimal results across both scene flow (EPE: 0.452, AccR: 0.443) and depth metrics (AbsR-r: 0.111, $\delta_1 - r$: 0.927).

3D Prior	Scene Flow Estimation				Depth Estimation			
	EPE↓	AccS↑	AccR↑	Out↓	AbsR-r↓	δ_1 -r↑	AbsR-m↓	δ_1 -m↑
Ours (scratch)	1.071	0.420	0.442	0.957	0.353	0.433	0.547	0.049
Ours (DUS3R [102])	0.588	0.378	0.408	0.896	0.121	0.887	0.233	0.423
MASt3R [47]	3.708	0.264	0.267	0.999	0.108	0.929	0.245	0.288
Ours (MASt3R [47])	0.452	0.398	0.443	0.873	0.111	0.927	0.236	0.345

Table 4. **Ablation over Joint Estimation Pipelines.** Verify the effect of 3D Prior and Offset Heads on KITTI. In the table ‘Ours (w)’ is our model initialized with the weights of method ‘w’.

Data	Scene Flow Estimation				Depth Estimation			
	EPE↓	AccS↑	AccR↑	Out↓	AbsR-r↓	δ_1 -r↑	AbsR-m↓	δ_1 -m↑
<i>exclude</i>	0.641	0.392	0.431	0.899	0.116	0.922	0.256	0.237
<i>specific</i>	0.569	0.317	0.393	0.911	0.090	0.925	0.580	0.095
<i>all</i>	0.452	0.398	0.443	0.873	0.111	0.927	0.236	0.345

Table 5. **Ablation over Data Recipe** on KITTI. *all*: using all datasets for training. *exclude*: using all datasets, except for train set of VKITTI2. *specific*: only using train set of VKITTI2.

B.2. Data Recipe is Key for Generalization

In Tab. 5, we explore how the datasets used in training affect the performance on KITTI. We compare our method performance with three training strategies: training on all the datasets (all), training on all but VKITTI2 (exclude), and training only on VKITTI2 (specific). Note that none of these strategies train on KITTI. Unsurprisingly, training with all datasets yields the best overall performance for both scene flow and depth. However, when omitting VKITTI2, which is the only driving dataset use, we maintain robust performance (EPE: 0.641, AbsR-m: 0.256), which demonstrates the generalization capabilities gained with diverse data exposure.

B.3. Reference coordinate frame

DUS3R and MASt3R make predictions of pointmaps from pairs of images, where both sets of points are predicted in the coordinate frame of the first camera C_1 . As scene flow estimation does not typically assume camera poses, it is defined as the (field of) vector from a 3D point in the first camera frame C_1 at time t_1 to a 3D point in the second camera frame C_2 at time t_2 . This difference of output reference frames—either always predicting in C_1 or from C_1 into C_2 —raises the question of whether the reference coordinate frame is important for prediction accuracy. This is especially true given that we fine tune the DUS3R network that operates solely in C_1 .

We ran an experiment to change the reference scene flow coordinate frame for our output scene flow: either 1) from C_1 into C_2 , 2) from C_1 to C_1 (sometimes called *rectified scene flow*), or 3) within a world coordinate frame. Scene flow training data labels are defined from C_1 to C_2 as in 1), so to produce the vector from C_1 to C_1 we must reproject the 3D end point of the vector into C_1 ’s reference frame using

Table 6. **Changing reference coordinate frame for the end point of scene flow.** For synthetic data with known camera poses from which to accurately translate coordinate frames for training data and evaluation, there is no clear gain from any of the reference frames (VKITTIv2, Spring). For real-world KITTI data, camera poses may be in error, and we see large increases in scene flow error when attempting to train and evaluate on scene flow data in a different reference frame.

Reference frame	Scene Flow Estimation				Depth Estimation			
	EPE↓	AccS↑	AccR↑	Out↓	AbsR-r↓	δ_1 -r↑	AbsR-m↓	δ_1 -m↑
VKITTI2 Dataset [11]								
<i>Known camera poses</i>								
World	0.154	0.744	0.830	0.511	0.140	0.856	0.222	0.682
Camera 1	0.202	0.808	0.886	0.449	0.139	0.858	0.210	0.711
Camera 2	0.190	0.780	0.876	0.484	0.137	0.859	0.236	0.634
Spring Dataset [65]								
<i>Known camera poses</i>								
World	0.010	0.986	0.998	0.812	0.265	0.600	1.132	0.043
Camera 1	0.012	0.990	1.000	0.811	0.272	0.594	0.716	0.103
Camera 2	0.013	0.989	0.999	0.813	0.280	0.597	0.679	0.119
KITTI [67]								
<i>Estimated camera poses</i>								
World	2.637	0.268	0.271	0.995	0.110	0.928	0.212	0.546
Camera 1	4.202	0.251	0.253	0.992	0.108	0.928	0.214	0.519
Camera 2	0.452	0.398	0.443	0.873	0.111	0.927	0.236	0.345

known ground truth camera poses. When computing metrics like end point error or accuracy against ground truth scene flow from C_1 to C_2 , this transformation is also necessary. For synthetic datasets like Spring and VKITTI2, the transformation is simple as camera poses are known. For VKITTI2, the camera poses must be estimated and may be in error.

Table 6 shows that the choice of coordinate frame is not significantly important when evaluated on Spring and VKITTI2, with any reference frame scoring approximately similarly. This suggests that the pretrained backbone can be successfully fine tuned with scene flow data and our training scheme for any coordinate frame. For VKITTI2, we observe large drops in performance as the reference frame changes. We attribute this to errors in the estimated camera poses, which affect training and metric evaluation.

B.4. Additional quantitative evaluation

We show our method’s superiority with comparison with different checkpoints of previous monocular scene flow methods in Tab. 7.

KITTI [67] (Real)									
Method	Scene Flow Estimation				Depth Estimation				
	EPE↓	AccS↑	AccR↑	Out↓	AbsR-r↓	δ_1 -r↑	AbsR-m↓	δ_1 -m↑	
<i>Ours</i>	0.452	0.398	0.443	0.873	0.111	0.927	0.236	0.345	
Self-Mono-SF [30]-kitti-train	0.454	0.345	0.435	0.853	0.100	0.905	0.105	0.879	
In Self-Mono-SF [30]-kitti-eigen	0.517	0.392	0.457	0.870	0.085	0.929	0.089	0.917	
OpticalExpansion [109]-kitti-train	2.703	0.357	0.366	0.970	0.132	0.871	0.529	0.172	
OpticalExpansion [109]-kitti-trainval	2.682	0.359	0.367	0.967	0.132	0.871	0.529	0.172	
<i>Ours-exclude</i>	0.641	0.392	0.431	0.899	0.116	0.922	0.256	0.237	
Out OpticalExpansion [109]-driving	2.537	0.348	0.363	0.968	0.132	0.871	0.529	0.172	
OpticalExpansion [109]-robust	2.702	0.359	0.366	0.969	0.132	0.871	0.529	0.172	
VKITTI2 [11] (Real)									
Method	Scene Flow Estimation				Depth Estimation				
	EPE↓	AccS↑	AccR↑	Out↓	AbsR-r↓	δ_1 -r↑	AbsR-m↓	δ_1 -m↑	
<i>Ours</i>	0.190	0.780	0.876	0.484	0.137	0.859	0.236	0.634	
Self-Mono-SF [30]-kitti-train	0.294	0.694	0.751	0.589	0.244	0.568	0.224	0.589	
In Self-Mono-SF [30]-kitti-eigen	0.373	0.688	0.738	0.666	0.200	0.668	0.189	0.669	
OpticalExpansion [109]-kitti-train	1.879	0.653	0.663	0.947	0.194	0.727	0.203	0.746	
OpticalExpansion [109]-kitti-trainval	1.845	0.655	0.664	0.946	0.194	0.727	0.203	0.746	
<i>Ours-exclude</i>	0.409	0.727	0.772	0.696	0.144	0.836	0.168	0.778	
Out OpticalExpansion [109]-driving	1.809	0.654	0.662	0.946	0.194	0.727	0.203	0.746	
OpticalExpansion [109]-robust	1.915	0.654	0.662	0.958	0.194	0.727	0.203	0.746	
Spring [65] (Synthetic)									
Method	Scene Flow Estimation				Depth Estimation				
	EPE↓	AccS↑	AccR↑	Out↓	AbsR-r↓	δ_1 -r↑	AbsR-m↓	δ_1 -m↑	
In <i>Ours</i>	0.013	0.989	0.999	0.813	0.280	0.597	0.679	0.119	
<i>Ours-exclude</i>	0.014	0.992	1.000	0.787	0.294	0.599	0.682	0.130	
Self-Mono-SF [30]-kitti-train	1.005	0.251	0.328	0.880	0.501	0.353	0.784	0.044	
Self-Mono-SF [30]-kitti-eigen	0.717	0.272	0.365	0.895	0.532	0.344	0.772	0.050	
Out OpticalExpansion [109]-driving	0.029	0.873	0.971	0.805	0.430	0.468	0.804	0.004	
OpticalExpansion [109]-kitti-train	0.038	0.849	0.935	0.799	0.430	0.468	0.804	0.004	
OpticalExpansion [109]-kitti-trainval	0.027	0.916	0.967	0.800	0.430	0.468	0.804	0.004	
OpticalExpansion [109]-robust	0.016	0.969	0.995	0.801	0.430	0.468	0.804	0.004	

Table 7. Comparison with Monocular Scene Flow Methods.

<i>Self-Mono-SF</i> [30]-kitti-train:	Trained on KITTI, train split;
<i>Self-Mono-SF</i> [30]-kitti-eigen:	Trained on KITTI, eigen split;
<i>OpticalExpansion</i> [109]-driving:	Trained on Driving [63];
<i>OpticalExpansion</i> [109]-kitti-train:	Trained on Driving [63], and then finetune on KITTI, train split;
<i>OpticalExpansion</i> [109]-kitti-trainval:	Trained on Driving [63], and then finetune on KITTI, trainval split;
<i>OpticalExpansion</i> [109]-robust:	Trained for the Robust Vision Challenge.